Published in final edited form as:

*Nat Mater*. 2009 October ; 8(10): 843–849. doi:10.1038/nmat2512.

# Spotted vesicles, striped micelles, and responsive Janus assemblies induced by ligand binding

**David A. Christian**[1,2], **Aiwei Tian**[1,2,3], **Wouter G. Ellenbroek**[1,4], **Ilya Levental**[1,5], **Karthikan Rajagopal**[1,2], **Paul A. Janmey**[1,4,5], **Andrea J. Liu**[1,4], **Tobias Baumgart**[1,3,4], and **Dennis E. Discher**[1,2,4,5,*]

[1]Laboratory for Research on the Structure of Matter, University of Pennsylvania, Philadelphia, Pennsylvania 19104

[2]Chemical & Biomolecular Eng'g., University of Pennsylvania, Philadelphia, Pennsylvania 19104

[3]Chemistry, University of Pennsylvania, Philadelphia, Pennsylvania 19104

[4]Physics & Astronomy, University of Pennsylvania, Philadelphia, Pennsylvania 19104

[5]Bioeng'g Graduate Groups, University of Pennsylvania, Philadelphia, Pennsylvania 19104

## Abstract

Selective binding of multivalent ligands within a mixture of polyvalent amphiphiles provides, in principle, a mechanism to drive domain formation in self-assemblies. Divalent cations are shown here to crossbridge polyanionic amphiphiles that thereby demix from neutral amphiphiles and form spots or rafts within vesicles as well as stripes within cylindrical micelles. Calcium and copper crossbridged domains of synthetic block copolymers or natural lipid ($PIP_2$, phosphatidylinositol-4,5-bisphosphate) possess tunable sizes, shapes, and/or spacings that can last for years. Lateral segregation in these 'responsive *Janus* assemblies' couples weakly to curvature and proves restricted within phase diagrams to narrow regimes of pH and cation concentration that are centered near the characteristic binding constants for polyacid interactions. Remixing at high pH is surprising, but a theory for Strong Lateral Segregation (SLS) shows that counterion entropy dominates electrostatic crossbridges, thus illustrating the insights gained into ligand induced pattern formation within self-assemblies.

### Keywords

lipids; block copolymers; polymersomes; rafts; domains; vesicles; worm-like micelles; polyelectrolyte



*email: discher@seas.upenn.edu.

**AUTHOR CONTRIBUTIONS** D.A.C., A.T., I.L., P.A.J., T.B., and D.E.D. designed experiments and analyzed data; D.A.C., A.T., I.L., performed experiments; W.G.E, A.J.L. developed the SSL theory; K.R. contributed new reagents; and D.A.C., W.G.E., A.J.L., T.B., and D.E.D. wrote the paper.

Supplementary information accompanies this paper on www.nature.com/naturematerials

Amphiphiles of suitable proportions will self-assemble in water into vesicles as well as high curvature micelles1–4, and *within* such assemblies controlled demixing to form fully segregated '*Janus*' assemblies has been postulated 5–7. Here we show that divalent cations can drive meso-scale domain formation within assembled mixtures of neutral and anionic polymer amphiphiles, including both synthetic polymers and highly charged lipids. '*Responsive Janus* assemblies' that form only upon addition of a ligand could enable new approaches to higher order assemblies8, delivery of drugs9, and hierarchical patterning10, 11. To date, only nano-scale domains have been reported in block copolymer mixtures, driven by fluorinated or crystallizing diblocks 10, 12, 13. In lipid bilayers, micron-sized domains have been documented, but domains have generally been induced by a mismatch of lipid acyl chains 14–16. Ion-induced domain formation in lipid vesicles is of interest in cell signaling and other dynamic membrane processes17, but past results using lipids of net change −1 or less appear highly controversial 18, 19 – possibly because lipid systems are soft and highly dynamic.

Charged block copolymers can generate morphologies that are stable but tunable after polymer synthesis by varying pH and salt concentration 4, 20. Polymer-based vesicular 'polymersomes' and worm-like micelles are mechanically tough compared to lipid assemblies, while polymers also provide broad choices in chemistry and bilayer dimensions ($d$ ~ 10 – 100 nm in Fig. 1-inset) with properties tailored for insight and application1–4. The stability of polymer assemblies generally increases with molecular weight $M_n$, exhibiting lifetimes (~ $e^{Mn}$) that can reach years and that therefore permit equilibration. With mixtures of polyanionic and neutral amphiphiles, we hypothesized that cation crossbridging of the polyanions – including both block copolymers and some highly charged lipids – would be sufficiently strong to segregate laterally into stable mesoscopic 'gel' domains that would couple only weakly to curvature effects.

## Spotted Vesicles and Calcium-gelation

We initially studied mixtures of two polymer amphiphiles. A relatively symmetric poly(acrylic acid)-polybutadiene copolymer denoted **AB1** ($M_n$ = 10,050 g/mol, with hydrophilic fraction, $f \approx 0.50$) yields polymersomes and micelles as a function of pH and salt, whereas the non-ionic poly(ethylene oxide)-polybutadiene denoted **OB18** ($M_n$ = 10,400 g/mol, $f$ ~ 0.35) yields coexisting cylinders and vesicles independent of pH and salt. When OB18 is labeled with a rhodamine fluorophore (OB18*) and mixed with unlabeled AB1 in various proportions, calcium-induced domains or rafts can be clearly seen in almost all giant vesicles (Fig. 1a–c). Polymersomes were immobilized by aspiration into a micropipette, which not only facilitated $z$-stack imaging by laser scanning confocal microscopy (LSCM) but also established that the membranes are stable under applied tension. Analysis of the area fraction of AB1 domains corresponds closely to the copolymer blend ratio (supporting information Table S1); for example, 25% AB1 gave a total area fraction of 0.22 ± 0.10 (n = 5 vesicles). The low diffusivity of OB18 1 minimizes drift effects that have frustrated similar high resolution studies of lipid vesicles. Moreover, domains here could be visualized for years after vesicle formation, and yet domains also dissipate within minutes upon addition of a calcium chelator (Fig. S1), indicating that calcium induces thermodynamically stable phase separation.

Strong lateral segregation (SLS) of the two copolymers was confirmed by simultaneous two-color imaging of vesicles made with both OB18* and a fluorescently-labeled AB1 (denoted AB1*) (Fig. 1d). Analysis of the fluorescence intensity of each color in both phases reveals a >3-fold enrichment of OB18* in OB18-rich domains and a similar enrichment of AB1* in AB1-rich domains – although this is probably a minimum estimate that is limited by optics. The importance of calcium suggests that this divalent cation acts as a crossbridge between polyanionic AB1 chains, and while the electrostatic basis for domain formation might seem intuitive we show below that domain formation occurs only in a highly restricted regime of pH and ion concentration. To assess the possible generality of the effect, a highly anionic and fluorescently-labeled lipid phosphatidylinositol-4,5-bisphosphate ($PIP_2$), was added to the polymer film; this, too was found enriched in the AB1-rich domains of vesicles (Fig. 1e). In a second test of the electrostatic interactions, another divalent cation, copper(II) transition metal, was added and indeed found to cause domain formation, although the domains appear more fractured (Fig. 1f, Fig. S3), probably as a result of the stronger interactions between transition metals and PAA21, 22. The weaker crossbridging of AB1 by calcium apparently led to phase separation but not strong gelation, so that AB1 molecules can diffuse to form circular domains that coarsen with time in minimizing boundary energy. Indeed, a hint of coarsening was seen in our initial studies with a few fully segregated “Janus” vesicles having nearly homogeneous and distinct hemispheres (Fig. 1g).

To assess coarsening and perhaps gain control over domain size, we extended the hydration time. The results above were obtained by making polymersomes with overnight hydration of polymer films heated to 60 °C; longer hydration times indeed give larger domains which coarsen until there is only ~ 1 domain per (15 $\mu m^2$ vesicle) after roughly 40 hours (Fig. 2). The total area fraction of domains per vesicle remains constant at the initial mixing ratio, independent of hydration time, indicating that phase separation is always complete. Calcium-responsive Janus vesicles thus controllably form on time scales of days and prove stable for far longer.

In using micropipette aspiration to immobilize vesicles, we observed that the extent of aspirated membrane within the pipette depended on the phase being aspirated. Aspirated projections of the continuous OB18* phase (Fig. 1a,b) were seen at pressures of 70 Pa, whereas no significant projection could be obtained in the continuous AB1 phase (Fig. 1c) at pressures up to 500 Pa. The difference in domain deformability seemed consistent with an increase in membrane stiffness caused by calcium-mediated bridging between polyanionic chains, but to study this in more detail, we aspirated pure AB1 polymer vesicles and determined an effective rigidity $E_{app}$ for the membranes as a function of pH and calcium concentration23. For gel networks21 or polymer brushes composed of weak polyelectrolytes like PAA22, increased ionization results in a greater calcium bridging effect evident in gel or brush volume changes. Indeed, we find that at a constant calcium concentration of 0.1 mM (Fig. 3a), membrane rigidity increases 20-fold with ionization from $E_{app}(pH_0\ 4) \approx 0.6$ mN/m to $E_{app}(pH_0\ 6) \approx 12.7$ mN/m, consistent with a 100-fold decrease in $[H^+]$ across PAA’s $pK_a \sim 5$. The low-pH polymersomes also exhibit a spherical contour outside of the pipette, typical of liquid-phase vesicles, whereas the stiffer, high-pH vesicles flatten near the pipette mouth as they buckle and distort, similar to covalently crosslinked solid

polymersomes23. Whether fluid or gel-like, these vesicles sustain membrane tensions and strains far above those achievable with lipid membranes. The stability is due to polymer membranes being several-fold thicker than lipid bilayers ($d \sim 4$ nm) rather than being intrinsically stiffer.

With increasing pH, AB1 membranes become negatively charged, which promotes calcium bridging and membrane rigidification (Fig. 3b). However, $E_{app}$ is more sensitive to calcium concentration than to pH (Fig. 3c). The effective rigidity in either case is fit to a power law form:

$$E_{app} = A([\text{ion}]/K)^{a} \quad \text{Eq. 1}$$

where [ion] is either $[H^+]$ or $[Ca^{2+}]$, $K$ is the relevant dissociation constant, $A$ is a pre-factor, and a is a power law exponent. Best-fit parameters indicate stronger scaling for calcium than for protons ($a_{Ca} = 2.5$ versus $|a_{H+}| = 0.34$). Calcium also gives much stronger scaling than the linear scaling of polymer network rigidity that is expected with simple covalent crosslinkers; the enhancment implicates cooperative calcium interactions, perhaps via calcium-induced increases in brush ionization22. Based on these results, domains in the spotted polymersomes at low pH and only moderate $[Ca^{2+}]$ are likely to be liquid-like or weak gels – consistent with both circular domain shapes and also the noted resistance to aspiration.

Fluorescence Recovery After Photobleaching (FRAP) confirmed gelation in the 100% AB1 system. A cationic fluorescent dye (DiO:C18) mixed into the AB1 membranes allowed photobleaching of a small circular area (radius $\rho \sim 0.5$ μm) on top of individual vesicles, and the time-dependent fluorescence recovery (Fig. 3d) gave characteristic diffusion times, $\tau_D$, that proved small at very low pH but immeasurably long at $pH_0 = 5$. The diffusivity $D = \rho^2/(4\tau_D)$ for the cationic probe (Fig. 3e) is nearly linear with proton concentration in the transition regime ($pH_0 \sim 4$) even when fitted to a form similar to that for rigidity (Eq.1), i.e. $D = B\,([H^+]/K)^b$ ($b \approx 0.9$ and $B = 9\times10^{-5}$ μm$^2$/s). FRAP studies with a neutral hydrophobic dye showed no diffusivity dependence on pH or calcium, confirming that the gelation effects were confined to the PAA brush (Fig. S4). Based on the measured pH-dependence of membrane rigidity (Fig.3b: $|a_{H+}| = 0.34$), the ratio of mobility/rigidity exponents, $|b/a| \approx 2.5$, is much larger than that seen with dynamically crosslinked entanglements in bulk polymers for which $|b/a| \approx 0.55$ 24. Electrostatic interactions are apparently more effective in slowing diffusion of AB1 chains than at rigidifying the brush, whereas polymer entanglements have the opposite effect.

## Striped Cylinders

Poly(acrylic acid) at high pH becomes so highly charged that electrostatic repulsion in AB1 curves the core-brush interface and generates cylindrical micelles20. Mixtures with OB18* behave no differently – except for the narrow range of pH and calcium in which cylinders appear striped (Fig. 4a). Image overlays clearly show that phase-separated cylinders are both continuous and flexible, with a persistence length of 5–10 μm that is similar to pure systems20.

Alternating dark and fluorescent segments are 0.3–1 μm in length, and their area fractions are in approximate proportion to the blend ratios of AB1:OB18* (Fig. 4b; Table S1). Striped nano-scale demixing with strongly segregating block copolymers has been predicted for small diameter cylinders25 and has been observed by electron microscopy both for fluoropolymer-based triblock copolymers10 and for semicrystalline diblocks in epitaxial growth of single nano-stripes13. Here, calcium-mediated interactions yield periodic meso-scale domains that alternate in a periodic fashion that is correlated at length scales up to 17 μm (Fig. 4c, Fig. S5). Distributions of fluorescent domain length $L$ for all compositions fit well ($R^2$ _≥ 0.95) to a linear growth model with termination by combination or coarsening, $P(L) \sim L \exp(2L/L_n)$ (Fig. 4d), giving a characteristic length $L_n$ that proves linear in copolymer ratio (Fig. 4d, **inset** $R^2 = 0.96$)) and that predicts tunable, ligand-dependent domain sizes from nm to μm. The uniformity in the width of the stripes could be due to the kinetics of domain formation. For example, if the AB1-rich domains have a lower spontaneous curvature than the OB18 domains, then phase separation might proceed via a periodic peristaltic mode26. Coarsening of domains is unlikely in the quasi-1D geometry of a cylinder micelle, since there is little decrease in interfacial area with coarsening.

## The Phase Diagram

Systematic mapping of the pH- and calcium-dependent phase diagram for the 25:75 copolymer mixture (Fig. 5a, Fig. S6a) expands otherwise similar morphological studies with pure AB120, (shaded gray with AB1 morphology designated as spherical micelles (S), worm-like micelles (W), and vesicles (V)), and pinpoints a relatively narrow regime of Strong Lateral Segregation (SLS). From pH 3.5 to 5.5 and at $[Ca^{2+}]$ = 0.025 to 0.4 mM this stable window of SLS corresponds to chemical potential widths of just ~ 2–5 $k_BT$ (= $k_BT$ $\log n\{[ion]_{max}/[ion]_{min}\}$). Spotted polymersomes dominate at intermediate pH and calcium, but increases in pH and calcium destabilize the membranes and generate “squids” of vesicle-connected cylinder micelles. Higher pH plus high calcium leads, as predicted27, to re-entrant micelles that are likely over-charged, so that their net charge is positive (Fig. S6b). As with pure AB1, the blend also exhibits a morphological vesicle-cylinder transition – striped cylinders rather than spotted polymersomes form by film rehydration – with a slight decrease in calcium and an increase in pH. The fluid-to-gel transition of pure AB1 polymersomes (filled circles) and worm-like micelles (filled squares) is indicated by the blue (fluid) and orange (gel) points in the phase diagram. The dashed line provides an estimate of this transition, and clearly indicates that aqueous conditions must be permissive for AB1 gels to achieve phase separation in these assemblies.

The generality of the phase diagram was tested with initial studies of giant unilamellar vesicles (GUVs) containing fluorescent-$PIP_2$, which is amongst the most anionic of natural lipids (−4 charge near pH 7) and which is also a major signaling lipid in the cytoplasmic leaflet of cell membranes28. GUVs composed of 95% DOPC, 4.9% $PIP_2$, and 0.1% BodipyTR-$PIP_2$ and formed by electroformation at 37 °C appeared homogeneous at pH 7.5 (Fig. S7a). The addition of lipid GUVs to calcium-containing buffer ($[Ca^{2+}]$ = 500 μM) induced domains enriched in $PIP_2$ within minutes (Fig. S7b). Domain formation was reversed with addition of a calcium chelator (Fig. S7c). GUVs incubated in pH = 3 buffer (where $PIP_2$ has a net charge near -1) appeared homogeneous (Fig. S7d), and no domains

were visible in GUVs incubated at pH = 3, [$Ca^{2+}$] = 500 μM (Fig. S7e). These lipid results show that calcium induces phase separation in mixed lipid vesicles as well as mixed polymer vesicles, and also emphasize that SLS occurs only in a narrow region in pH.

## Strong Lateral Segregation Theory

A simple equilibrium model for SLS was derived based on calcium-mediated attraction between polyanionic chains. While attractions, or crossbridges, lead to gelation (above the blue dashed line in Fig. 5a), a medley of competing effects restricts calcium-mediated lateral segregation to an even narrower window of calcium concentration and pH. A high net charge favors mixing, since electrostatic repulsion is high in domains rich in polyanion. As a result, SLS does not occur at low [$Ca^{2+}$], where there is little counterion condensation and the net charge of the aggregates is highly negative. The same effect prevents segregation at high [$Ca^{2+}$], where the charge apparently inverts to a high net positive charge on the aggregates. At high [$H^+$] (pH < p$K_a$ for PAA) few charged groups on the AB1 chains condense the $Ca^{2+}$ required to form crossbridges, therefore mixing is observed between the nearly neutral AB1 and neutral OB18. As [$H^+$] decreases, the system segregates with increasing crossbridging, but at lower [$H^+$], the entropic penalty associated with confining condensed $Ca^{2+}$ in PAA-rich domains increases, favoring mixing once again.

The free energy of the polymer-counterion system is calculated as a function of [$H^+$], [$Ca^{2+}$], and $\phi_A$, the local fraction of AB1 chains. The role of proton concentration is approximated as setting the “bare” charge of the AB1, using standard acid dissociation with a p$K_a$ ~ 5. Assuming either cylindrical or bilayer geometry, the ion concentrations in the hydrophilic brush of the assembly, $[H^+]_b$ and $[Ca^{2+}]_b$ are calculated using Oosawa’s two-state approach to counterion condensation29 including electrostatic screening. The counterion entropy density $s$ is given by

$$s \approx [\mathrm{H}^+]_\mathrm{b}\log_\mathrm{n}[\mathrm{H}^+]_\mathrm{b}+[\mathrm{Ca}^{2+}]_\mathrm{b}\log_\mathrm{n}[\mathrm{Ca}^{2+}]_\mathrm{b}. \quad \text{Eq. 2}$$

In a full electrostatic treatment, $Ca^{2+}$ crossbridges would arise naturally from counterion correlations beyond counterion condensation. Here, we treat them phenomenologically, so that the effective attraction energy per crossbridge, $E_c$, is a fitting parameter and the number of crossbridges is estimated by interpolating between two expected limiting behaviors. We assume that every $Ca^{2+}$ ion in the brush is close to a charged acrylic acid group. A crossbridge then forms when a $Ca^{2+}$ ion is also close to a second charged acrylic acid group in a second AB1 molecule. In regions of low $\phi_A$ (and hence low [$Ca^{2+}$]), this process is limited by the lateral fluctuations of the PAA chains, and the crossbridge density is $n_{c,small}$ = σ [$AA^-$][$Ca^{2+}$]. The prefactor σ depends on the chain lengths and brush density. If all densities are expressed in “per polymer chain” units then σ = 0.83, but our result is robust against variations of this parameter. At moderately large $\phi_A$, the crossbridge density is limited by the available $Ca^{2+}$ ions and is therefore $n_{c,large}$ = [$Ca^{2+}$]. We interpolate between the two limits by using $n_c=(n_{c,small}^{-3}+n_{c,large}^{-3})^{-1/3}$. The free energy includes a term for electrostatic self-energy and a Flory-Huggins-like term for the polymer chains. We determine the phase behavior using a double-tangent construction in $\phi_A$; the region in which phase separation occurs is enclosed by a solid black line in Fig. 5b for $E_c$ = 6 $k_BT$ for

vesicles with an AB1 fraction of 25%. The darkness within this region corresponds to the magnitude of a contrast function (0 when mixed, 1 when separated into domains of $\phi_A = 0$ and $\phi_A = 1$), and the dashed-dotted line corresponds to the contour with a contrast of 0.5. Such contours are plotted for worms (dotted) and vesicles (dashed-dotted) at AB1 fractions of 25%, 50%, 75% (Fig. 5c). These contours are superimposed on the experimental region of SLS. Note that this simple model cannot capture the charge inversion of the aggregates, which is a counterion correlation effect, and therefore cannot reproduce the high $[Ca^{2+}]$-end of the phase diagram correctly. The model also predicts phase separation at $[Ca^{2+}]$ significantly lower than observed experimentally. This result is not unexpected as phenomenological treatment of the electrostatics does not yet account for the cooperative interaction between calcium and PAA that was demonstrated here by rigidity measurements in which $a_{Ca}/a_{H+} \approx 7$ (Fig. 3b) exceeds the simple doubling expected from charge differences between $Ca^{2+}$ and $H^+$. However, close to the line of zero net charge, the present model reproduces the finite region of phase separation as observed in experiment.

Spotted polymersomes that were induced here by ligand binding constitute ‘responsive *Janus* structures’ that are highly tunable and stable even at near-physiological conditions (Fig. S8). SLS is only observed within a narrow window of solution conditions but in structures as diverse as polymer vesicles, lipid vesicles, and polymer cylinder micelles. The results indicate that the phenomenon is electrostatic in origin and can therefore occur in a wide range of systems: domain shape should be influenced by the addition of different metal cations (thus far copper and calcium but not sodium) or chelating agents (eg. EDTA) and domain formation should also occur with polybasic amphiphiles – although the limited biological application of positively charged assemblies (because they bind non-specifically to all negatively charged cell membranes and extracellular matrix) motivates further study of additional polyanionic assemblies with physiological cations such as calcium. The results here thus open up new routes to dynamic control over structural organization and functionalization within self-assembled synthetic materials.

## METHODS

Block copolymers of poly(ethylene oxide)-poly(butadiene) ($PEO_{80}$-$PBD_{125}$, $M_n$ = 10,400 g/mol, polydispersity PD = 1.1, designated OB18) or poly(acrylic acid)-poly(butadiene) ($PAA_{75}$-$PBD_{103}$, $M_n$ = 10,050 g/mol, PD = 1.1, designated AB1) were synthesized by standard polymerization or used as described20. Lipids were purchased from either Avanti Polar Lipids (SOPC, PIP2, NBD-PIP2) or Echelon Biosciences (BodipyFL-PIP2, BodipyTR-PIP2). The fluorophores TMRCA and Cascade Blue-ethylenediamine were purchased from Molecular Probes. Domain formation in polymersomes and worm-like micelles was visualized by dissolving fluorescently-labeled OB18 (OB18*) and AB1 polymers in chloroform and methanol and then drying to form a blended polymer film. The films were then hydrated in aqueous solution with known pH and calcium concentrations tuned by the addition of HCl and $CaCl_2$. OB18* was made by attaching tetramethyl rhodamine-5 carbonyl azide (TMRCA) to the hydroxyl end group of the PEO block. The modification involves TMRCA conversion to an isocyanate, which then modified the hydroxyl end group of PEO to a urethane. This end-group modification was carried out in toluene at 80°C for 12 hours. Excess, unreacted TMRCA dye was removed by a

recrystallization and washing process with methanol as verified by gel permeation chromatography. AB1* was made by attaching the amine-containing Cascade Blue to acrylic acid monomers along the backbone of the PAA chain using standard carbodiimide chemistry. Cascade Blue was added in 3 times excess of AB1 polymer, and unreacted dye was removed by dialysis and washes with water and methanol. Fluorescence microscopy and micropipette aspiration were performed as previously described15, 25 (See Methods in SI for additional details).

## Supplementary Material

Refer to Web version on PubMed Central for supplementary material.

## ACKNOWLEDGMENTS

The NSF-MRSEC at the University of Pennsylvania has provided primary support. Additional support from the NIH (D.E.D., P.A.J.), DOE (A.J.L.), and NSF (T.B.) is very gratefully acknowledged. We thank J.D. Pajerowski for his help with correlation length and periodicity analysis.

## REFERENCES

1. Discher DE, Eisenberg A. Polymer vesicles. Science. 2002; 297:967–973. [PubMed: 12169723]
2. Pochan DJ, et al. Toroidal triblock copolymer assemblies. Science. 2004; 306:94–97. [PubMed: 15459386]
3. Won YY, Davis HT, Bates FS. Giant wormlike rubber micelles. Science. 1999; 283:960–963. [PubMed: 9974383]
4. Zhang LF, Yu K, Eisenberg A. Ion-induced morphological changes in "crew-cut" aggregates of amphiphilic block copolymers. Science. 1996; 272:1777–1779. [PubMed: 8662482]
5. Fraaije J, van Sluis CA, Kros A, Zvelindovsky AV, Sevink GJA. Design of chimaeric polymersomes. Faraday Discuss. 2005; 128:355–361. [PubMed: 15658783]
6. Srinivas G, Pitera JW. Soft patchy nanoparticles from solution-phase self-assembly of binary diblock copolymers. Nano Lett. 2008; 8:611–618. [PubMed: 18189443]
7. Walther A, Muller AHE. Janus particles. Soft Matter. 2008; 4:663–668.
8. Glotzer SC, Solomon MJ. Anisotropy of building blocks and their assembly into complex structures. Nat. Mater. 2007; 6:557–562. [PubMed: 17667968]
9. Alexeev A, Uspal WE, Balazs AC. Harnessing Janus nanoparticles to create controllable pores in membranes. ACS Nano. 2008; 2:1117–1122. [PubMed: 19206328]
10. Cui HG, Chen ZY, Zhong S, Wooley KL, Pochan DJ. Block copolymer assembly via kinetic control. Science. 2007; 317:647–650. [PubMed: 17673657]
11. Wang H, Wang XS, Winnik MA, Manners I. Redox-mediated synthesis and encapsulation of inorganic nanoparticles in shell-cross-linked cylindrical polyferrocenylsilane block copolymer micelles. J. Am. Chem. Soc. 2008; 130:12921–12930. [PubMed: 18763779]
12. Li ZB, Kesselman E, Talmon Y, Hillmyer MA, Lodge TP. Multicompartment micelles from ABC miktoarm stars in water. Science. 2004; 306:98–101. [PubMed: 15459387]
13. Wang XS, et al. Cylindrical block copolymer micelles and co-micelles of controlled length and architecture. Science. 2007; 317:644–647. [PubMed: 17673656]
14. Baumgart T, Hess ST, Webb WW. Imaging coexisting fluid domains in biomembrane models coupling curvature and line tension. Nature. 2003; 425:821–824. [PubMed: 14574408]
15. Korlach J, Schwille P, Webb WW, Feigenson GW. Characterization of lipid bilayer phases by confocal microscopy and fluorescence correlation spectroscopy. Proc. Natl. Acad. Sci. U. S. A. 1999; 96:8461–8466. [PubMed: 10411897]
16. Veatch SL, Keller SL. Separation of liquid phases in giant vesicles of ternary mixtures of phospholipids and cholesterol. Biophys. J. 2003; 85:3074–3083. [PubMed: 14581208]

17. Clapham DE. Calcium signaling. Cell. 2007; 131:1047–1058. [PubMed: 18083096]
18. Haverstick DM, Glaser M. Visualization Of Ca-2+-Induced Phospholipid Domains. Proc. Natl. Acad. Sci. U. S. A. 1987; 84:4475–4479. [PubMed: 3474616]
19. Shoemaker SD, Vanderlick TK. Calcium modulates the mechanical properties of anionic phospholipids membranes. J. Colloid Interface Sci. 2003; 266:314–321. [PubMed: 14527454]
20. Geng Y, Ahmed F, Bhasin N, Discher DE. Visualizing worm micelle dynamics and phase transitions of a charged diblock copolymer in water. J. Phys. Chem. B. 2005; 109:3772–3779. [PubMed: 16851424]
21. Horkay F, Tasaki I, Basser PJ. Effect of monovalent-divalent cation exchange on the swelling of polyacrylate hydrogels in physiological salt solutions. Biomacromolecules. 2001; 2:195–199. [PubMed: 11749172]
22. Konradi R, Ruhe J. Interaction of poly(methacrylic acid) brushes with metal ions: Swelling properties. Macromolecules. 2005; 38:4345–4354.
23. Discher BM, et al. Cross-linked polymersome membranes: Vesicles with broadly adjustable properties. J. Phys. Chem. B. 2002; 106:2848–2854.
24. Gell CB, Graessley WW, Fetters LJ. Viscoelasticity and self-diffusion in melts of entangled linear polymers. J. Polym. Sci., Part B: Polym. Phys. 1997; 35:1933–1942.
25. Velichko YS, de la Cruz MO. Pattern formation on the surface of cationic-anionic cylindrical aggregates. Physical Review E. 2005; 72:041920.
26. Grason GM, Santangelo CD. Undulated cylinders of charged diblock copolymers. European Physical Journal E. 2006; 20:335–346.
27. Borisov OV, Zhulina EB. Reentrant morphological transitions in copolymer micelles with pHsensitive corona. Langmuir. 2005; 21:3229–3231. [PubMed: 15807557]
28. McLaughlin S, Murray D. Plasma membrane phosphoinositide organization by protein electrostatics. Nature. 2005; 438:605–611. [PubMed: 16319880]
29. Oosawa, F. Polyelectrolytes. New York: M. Dekker; 1971.

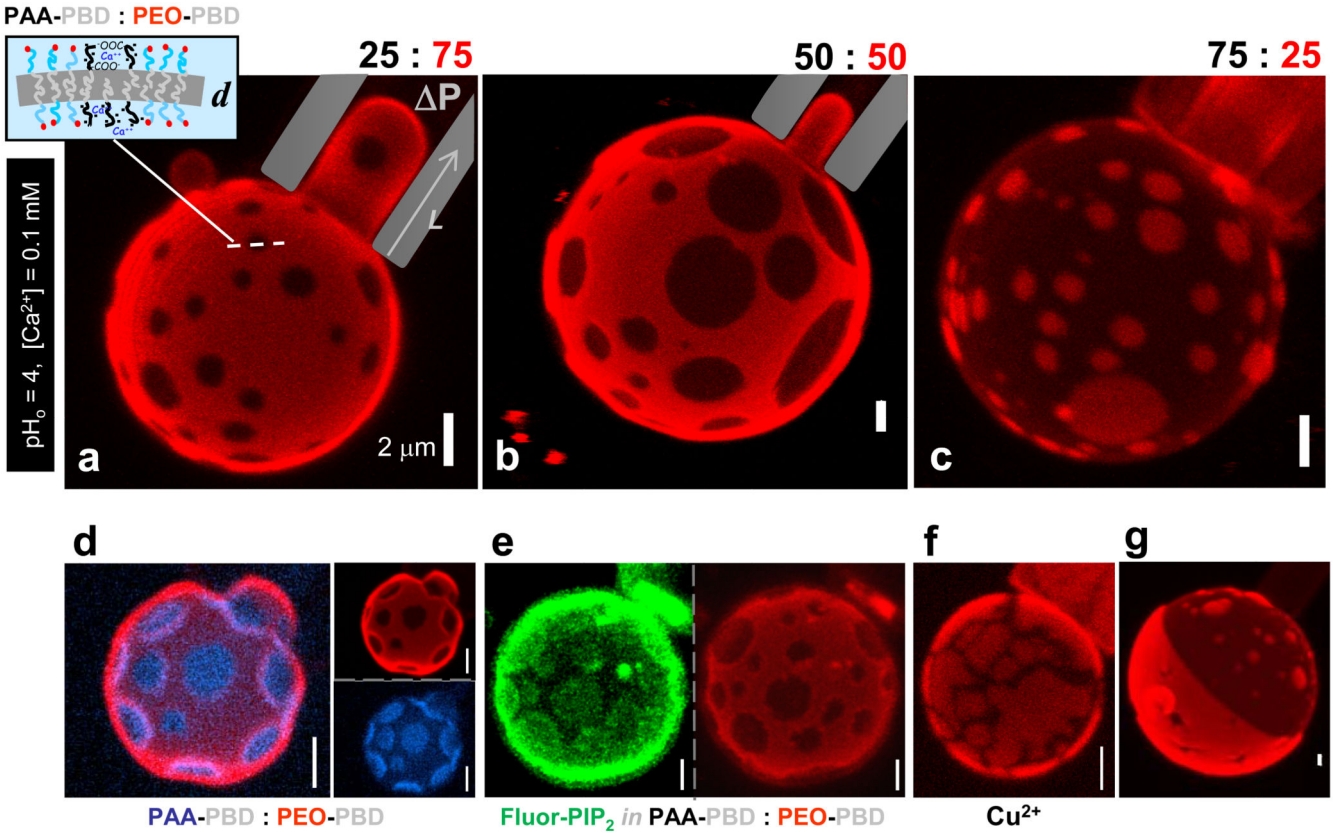


**Fig. 1. Spotted vesicles imaged by *z*-sectioning confocal microscopy while aspirated in micropipettes**

Cation-induced, lateral phase segregation of charged AB1 and neutral, fluorescently-labeled OB18* diblock copolymers formed at $pH_0$ 4, 0.1 mM calcium at **(a)** 25% AB1, **(b)** 50% AB1, and **(c)** 75% AB1. (**a**, inset): Schematic of phase-separated membrane of thickness *d*. **(d)** Two color micrograph of a phase separated polymersome (34% AB1, AB1:AB1* = 10:1) with individual red (OB18*) and blue (AB1*) channel micrographs to illustrate the extent of demixing. **(e)** Individual channels modified using an averaging smoothing filter to enhance contrast for a two color phase separated polymersome (50% AB1) with 2% PIP2-BodipyFL (green) enriched in dark AB1 domains and partially segregated from the OB18*-rich domains (red). Unmodified images and fluorescence intensity analysis of domains are shown in Fig. S2. **(f)** Phase separation of AB1 (50%) induced by copper(II) at $pH_0$ 3.5, 0.075 mM copper(II). **(g)** Janus polymersome resulting from domain coarsening in a 50% AB1 polymersome.

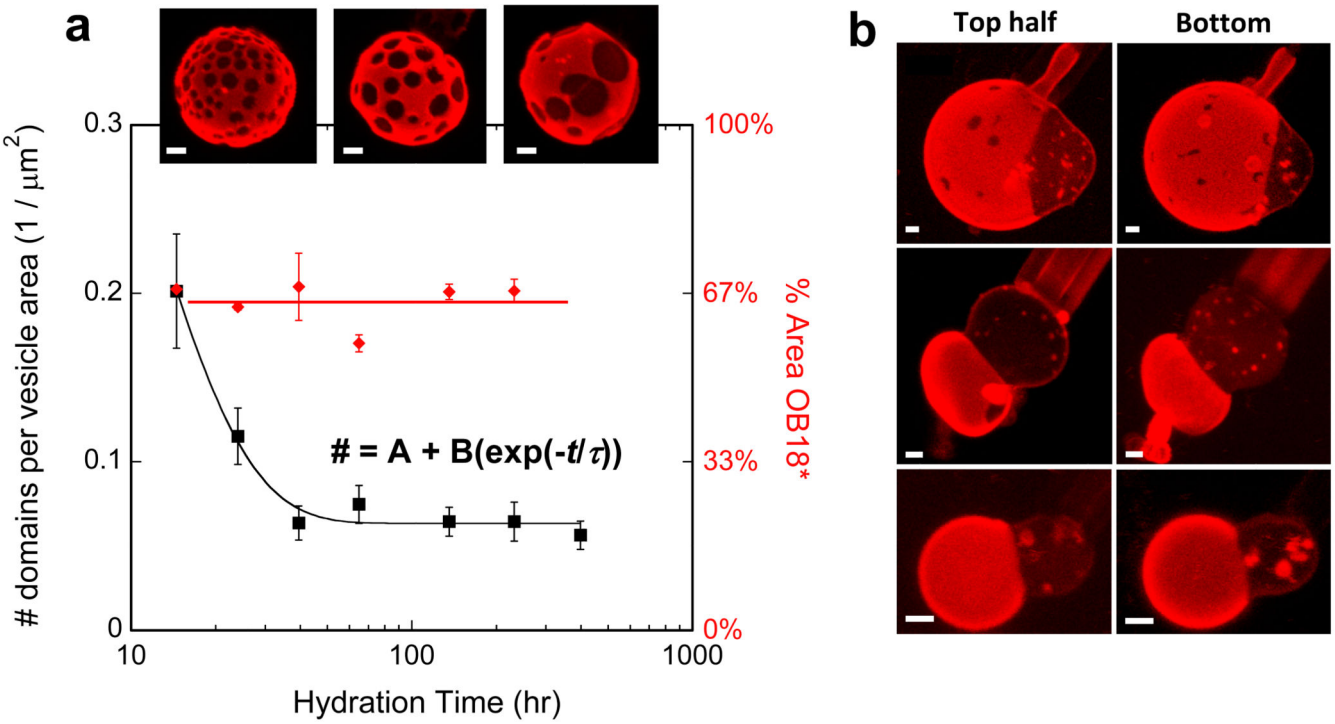


**Fig. 2. Controlled coarsening yields a majority of Janus-like Polymersomes**

Mixed films of 33:67 AB1 : OB18* were hydrated for the indicated times and vesicles were imaged at each time point to measure the domains per area (Avg ± S.E., $n \geq 3$ per time point). The coarsening of domains is shown to saturate by ~40 hr, but the % Area occupied by domains remains relatively constant throughout. As shown, a majority of polymersomes showed fully segregated domains after 2 or more days. Scale bars = 2 μm.

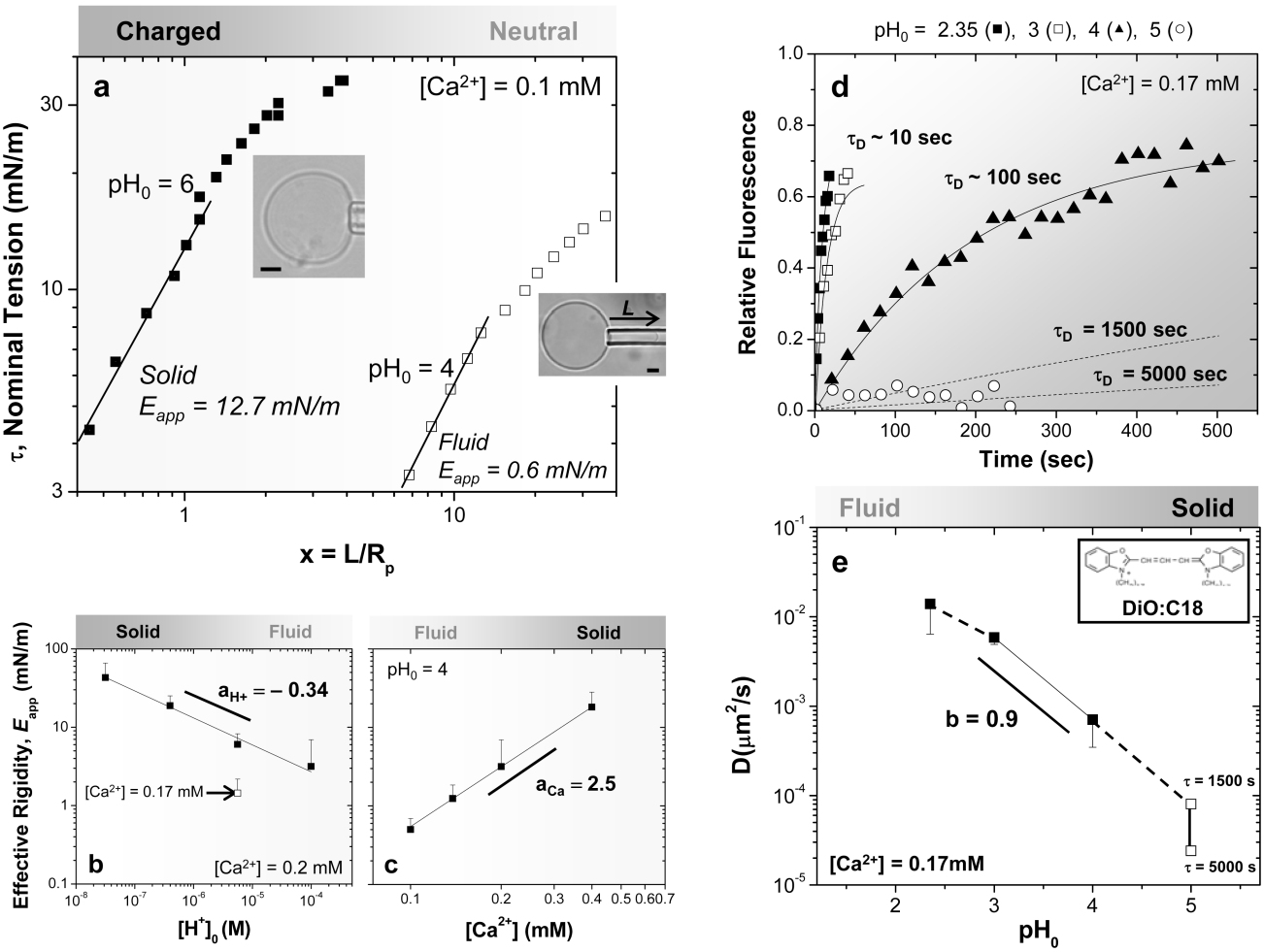


**Fig. 3. Fluid-gel transition of polyanionic polymersome brush with increasing pH or calcium**

**(a)** Effective elasticity of AB1 polymersomes hydrated at the indicated $Ca^{2+}$ and $pH_0$. Power law fits of the low strain regime provide a measure of Effective Rigidity $E_{app} = (\tau/x)^m$ in units of mN/m, which reveals a fluid, elastic membrane at $pH_0$ 4 ($m$ = 1) and inelastic deformation of a gel-like membrane at $pH_0$ 6 ($m$ = 1.25). Inset images respectively show spherical and non-spherical vesicle contours, consistent with fluid or solid-like behavior. **(b, c)** Power law fits of $E_{app}$ as a function of pH or calcium quantify the stiffening, and much stronger effects with calcium. Fitting with Eq. 1 yields for $[H^+]$: $a_{H+} = -0.34$, $A_{H+} = 6.0$ mN/m using a $pK_a = 5$ ($R^2 = 0.99$). For $Ca^{2+}$, $a_{Ca} = 2.5$ and $A_{Ca} = 0.002$ mN/m ($R^2 = 0.99$). **(d, e)** Relative fluorescence intensity versus time from FRAP of cationic DiO:C18 dye in AB1 polymersomes at varying $pH_0$. Fits provide the characteristic diffusion times $\tau_D$, and the calculated diffusion coefficients versus $pH_0$ are fit by a power law across the fluid-gel transition regime (solid line).

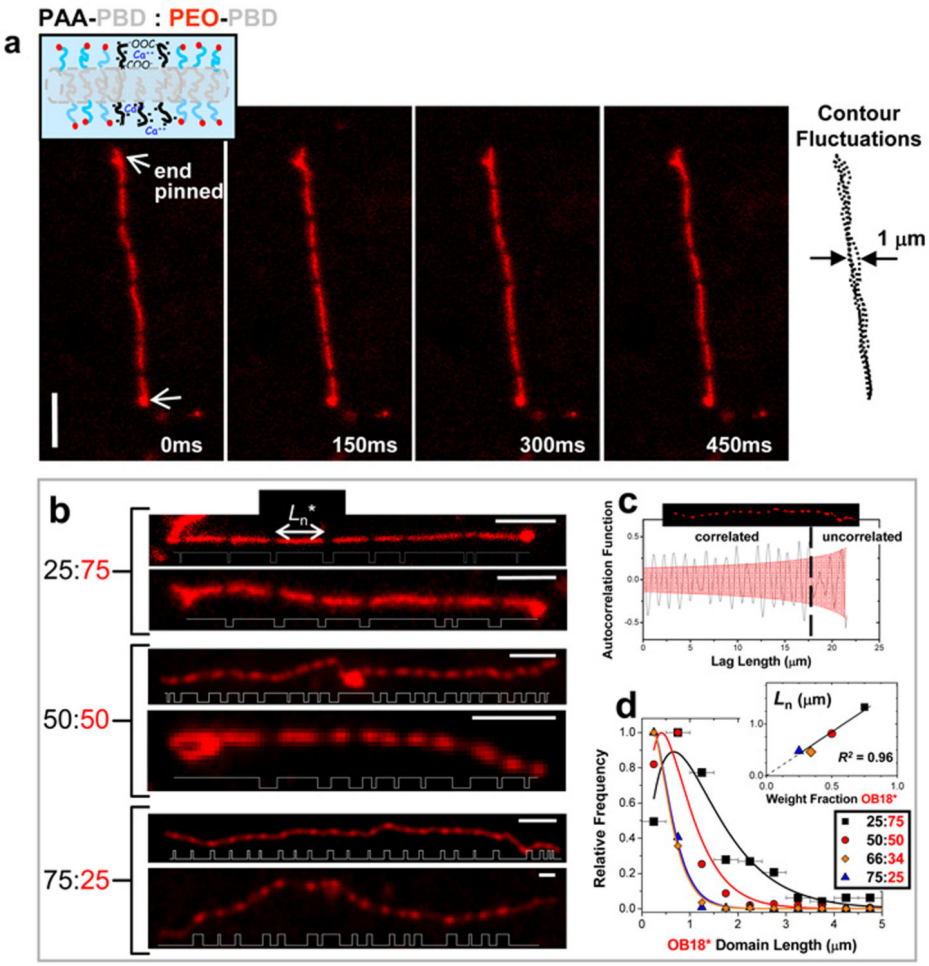


**Fig. 4. Striped cylinder micelles**

**(a)** Time sequence of a pinned, striped worm-like cylinder micelle formed with AB1:OB18* = 25:75 at $pH_0$ 4.5 and $[Ca^{2+}]$ = 0.05 mM; the micelle remains flexible as evident in the contour overlay. **(b)** Striped cylinder micelles formed at increasing AB1 fraction, although for any sample only about 10% of cylinders appeared definitively striped with multiple micron-sized bands. Plots of thresholded fluorescence intensity along the worm contour length highlight average domain size and periodicity. **(c)** The long range ordering of a single 75:25 worm micelle is at least 17 μm as determined by examining the autocorrelation of the backbone fluorescence intensity. **(d)** Domain lengths ($L$) of OB18* in striped cylinders at varying AB1 fraction are fit to a Zimm-Schulz model ($R^2 \geq 0.95$) in which the number average length, $L_n$*, scales linearly ($R^2 = 0.96$) with OB18* blend fraction (inset). Error bars represent bin sizes for $L$. Scale bar = 4 μm.

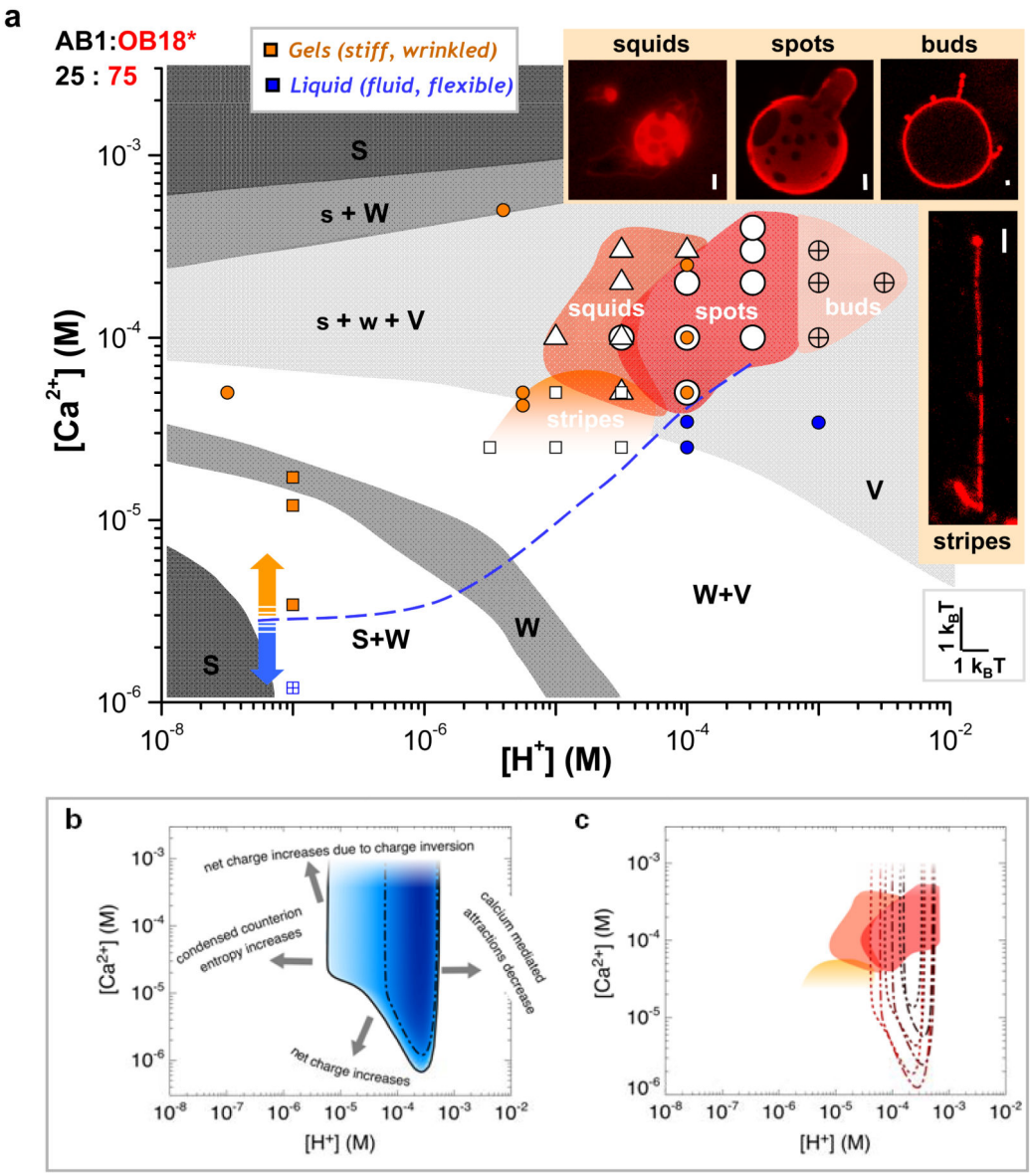


**Fig. 5. Phase diagram with narrow regime of domain formation for AB1:OB18* = 25:75 as observed experimentally and modeled theoretically**

**(a)** Systematic experimental phase diagram of domain formation for 25% AB1 is overlayed on the morphological phase diagram for pure AB1 (shown in gray; spherical micelles (S), worm-like micelles (W), and vesicles (V)) and displayed with points where experiments indicate whether pure AB1 polymersomes (colored circles) and worm-like cylinder micelles (colored squares) display fluid (blue) or gel (orange) characteristics. The calcium values in the morphological phase diagram were recalculated to correspond to the 0.025 mg/mL AB1 present in the blends used for domain formation while pH was converted to $[H^+]$. Four regions of interest were observed – buds, spots, squids, and stripes – as depicted in the inset images (scale bar = 2 μm). **(b)** The narrow window of domain formation observed experimentally is recapitulated using a theoretical model (solid line). Increasing blue intensity in the region of domains formation is representative of increasing contrast between

laterally segregated domains, where the dash-dotted line bounds the region where the contrast is larger than 50%. The dominating physical mechanisms for mixing are indicated with text. **(c)** Contours for 50% contrast are plotted for other constituent ratios where increasing line thickness represents an increase in AB1 fraction (25%, 50%, 75%) for cylinder micelles (dotted) and polymersomes (dash-dotted). These contours are plotted over the region of experimentally observed domain formation. The high calcium boundary is not obtained because the theoretical model does not capture charge inversion.